Formation and evolution of magnetic nanoparticles in borate glass simultaneously doped with Fe and Mn oxides

Cite as: J. Appl. Phys. **104**, 103917 (2008); https://doi.org/10.1063/1.3021289
Submitted: 08 August 2008 • Accepted: 04 October 2008 • Published Online: 26 November 2008

J. Kliava, I. Edelman, O. Ivanova, et al.

Formation and evolution of magnetic nanoparticles in borate glass simultaneously doped with Fe and Mn oxides

J. Kliava,[1] I. Edelman,[2] O. Ivanova,[2,a)] R. Ivantsov,[2] O. Bayukov,[2] E. Petrakovskaja,[2] V. Zaikovskiy,[3] I. Bruckental,[4] Y. Yeshurun,[4] and S. Stepanov[5]
[1]*CPMOH, Université Bordeaux, 1-CNRS UMR 5798, 33405 Talence Cedex, France*
[2]*Kirensky Institute of Physics, Siberian Branch of RAS, 660036 Krasnoyarsk, Russia*
[3]*Boreskov Institute of Catalysis, Siberian Branch of RAS, 630090 Novosibirsk, Russia*
[4]*Department of Physics, Bar-Ilan University, Ramat-Gan 52900, Israel*
[5]*S. I. Vavilov State Optical Institute, St. Petersburg 199034, Russia*

(Received 8 August 2008; accepted 4 October 2008; published online 26 November 2008)

Evolution of the phase state of paramagnetic additions at various stages of synthesis and subsequent thermal treatment of glasses of the system $Al_2O_3-K_2O-B_2O_3$ simultaneously doped with Fe_2O_3 and MnO is studied by means of a combination of experimental techniques: Faraday rotation (FR), electron magnetic resonance (EMR), transmission electron microscopy (TEM), Mössbauer spectroscopy, and magnetic measurements. Both FR and EMR show that magnetically ordered clusters occur already at the first stage of the glass preparation. In particular, for the ratio of the Fe and Mn oxides in the charge close to 3:2, fine magnetic nanoparticles are formed with characteristics similar to those of manganese ferrite. By computer simulating the EMR spectra at variable temperatures, a superparamagnetic nature of these nanoparticles is confirmed and their mean diameter is estimated as approximately 3.2 nm. In the thermally treated glasses larger magnetic nanoparticles are formed, giving rise to FR spectra, characteristic of magnetically ordered systems, and the EMR spectra different from those in as-prepared glasses but also showing superparamagnetic narrowing. The Mössbauer spectroscopy corroborates the manganese ferrite structure of the nanoparticles and indicates their coexistence in the ferrimagnetic and superparamagnetic states. The TEM shows the presence of polydisperse nanoparticles on the background of the glass matrix, and electron diffraction of a selected region containing larger particles indicates a crystal structure close to that of $MnFe_2O_4$. Energy-dispersive atomic x-ray spectra confirm that the major part of Fe and Mn introduced to the glass composition is gathered in the particles, with the concentration ratio close to 2:1, characteristic of bulk $MnFe_2O_4$. Magnetic hysteresis loops of samples subjected to an additional thermal treatment demonstrate a strong increase in the coercive force, remnant magnetization, and high-field magnetic susceptibility with temperature decrease. The consistent results obtained using various techniques demonstrate that the formation of nanoparticles with characteristics close to those of $MnFe_2O_4$ confers to these glasses magnetic and magneto-optical properties typical of substances possessing magnetic order. © *2008 American Institute of Physics*. [DOI: 10.1063/1.3021289]

I. INTRODUCTION

Nanomagnetism is both a fundamental and applied challenge. The magnetic properties observable on macroscopic scale are due to a very large number of atoms and, therefore, do not exist or are very different on a nanometric scale—for a single atom or molecule or for a cluster of a few atoms. The nanometric scale reveals some "exotic" properties, still poorly understood and hence poorly controlled during the nanoparticle synthesis. Meanwhile, the advent of nanomaterials is revolutionizing the technology, so understanding and control of their properties acquire a paramount importance. In particular, superparamagnetic systems consisting of magnetically ordered nanoparticles embedded in diamagnetic matrices attract great attention and a correlation between physical properties of the nanoparticles and of the matrix becomes one of the hottest problems of the physics (e.g., see Refs. 1–11).

Manganese ferrite is one of the compounds most frequently used in fabricating nanoparticle systems, both in powder state and embedded in various matrices.[4–7] The properties of materials containing magnetic nanoparticles depend on both intrinsic particle properties[3–6] and interparticle interactions.[8] Besides, the nanoparticle properties are greatly influenced by their surface or interface layers, where the environment of magnetic atoms differs from that in the core.[3,6] Therefore, different methods of sample preparation and different matrices used result in a large variety of magnetic characteristics observed in nanoparticle systems.

A special case of such systems is magnetic particles dispersed in glassy matrices (e.g., see Refs. 12–15). These materials are promising candidates for new magneto-optical data storage, optical fiber sensors,[16] optical isolators,[17,18] optical voltage sensors,[19] etc.

a)Electronic mail: osi@iph.krasn.ru.

Usually, in order to obtain magnetic particles, a high content (20–40 mass %) of paramagnetic oxides Fe_2O_3, MnO, or CoO must be added to the glass composition. However, some glass systems, partially devitrified by thermal treatment, elude this rule; indeed, nanoparticles of lithium ferrite $LiFe_5O_8$ in lithium borate glass containing less than 1 mass % Fe_2O_3 (Refs. 20 and 21) and nanoparticles of maghemite (γ-Fe_2O_3) in gel-silica glass with the Fe/Si molar ratio of 2% (Ref. 12) were identified by electron magnetic resonance (EMR).

In potassium-alumina-borate glasses subjected to thermal treatment under certain conditions, peculiarities of magnetic properties suggest the formation of ferrite particles at a paramagnetic oxide content of a few mass %.[22] Such glasses are characterized by a nonlinear magnetic field dependence of the magnetization with hysteresis and magnetic saturation. At the same time, they are transparent in the visible and near infrared spectral range and demonstrate a high value of the magneto-optical Faraday rotation (FR). Meanwhile, their magnetic properties largely depend on the thermal treatment conditions and relative and absolute concentrations of iron and manganese oxides. Understanding and control of these properties require a detailed study of correlations between the characteristics of individual nanoparticles, particle assemblies, and technological conditions of synthesis of such nanomaterials.

The aim of the present work is the monitoring of the phase state of paramagnetic additions—from diluted ions to clusters and nanoparticles—at various stages of synthesis and subsequent thermal treatment of glasses of the system 22.5 Al_2O_3–22.5 K_2O–55 B_2O_3 codoped with two transition metal oxides, Fe_2O_3 and MnO. In our previous study[23] using EMR and FR techniques we have described a series of glasses of this system containing, over 100 mass % of the basic composition, 1.5 mass % of Fe_2O_3, 0.0–0.9 mass % of MnO, and 0.0–0.5 mass % of GdO. In particular, we have shown that in this series directly after synthesis diluted Fe and Mn are present while under heat treatment at 560 °C during 2 h magnetically ordered nanoparticles are formed, predominantly including the iron ions. Here we report the results obtained with another series of samples of the same basic composition, containing, over 100 mass %, 3.0 mass % of Fe_2O_3 and MnO in the concentrations of 2.5 (samples 2 and 3) and 2.0 mass % (sample 1).

Using the EMR and FR we show that already in as-prepared samples iron and manganese are present both in diluted and in clustered state, forming magnetically ordered nanoparticles. The amount of each of these phases depends on the Mn concentration as well on the synthesis temperature. A model of the nanoparticles is proposed on the basis of computer simulations of their EMR spectra. For thermally treated glasses, using the EMR and FR, as well as transmission electron microscopy (TEM), Mössbauer effect, and magnetic measurements, we show that magnetic particles of a larger size are formed in this case and describe the intrinsic relation between the nanoparticles in the as-prepared and annealed samples.

TABLE I. MnO concentration, synthesis (T_s) and thermal treatment (T_t) temperatures, FR value α (for $\lambda = 800$ nm and magnetic field 0.5 T), relative remnant FR α_0/α, and coercive field B_c.

Sample	MnO (mass %)	T_s (°C)	T_t (°C)	FR (deg cm^{-1})	α_0/α	B_c (T)
			560	20.7	0.37	0.009
			600	2.9	0.02	0.007
1	2.0	1100	560+600	23.9	0.39	0.011
			560	13.7	0.32	0.012
			600	10.7	0.20	0.010
2	2.5	1000	560+600	12.3	0.31	0.010
			560	9.2	0.25	0.009
			600	10.7	0.30	0.011
3	2.5	1100	560+600	16.3	0.39	0.010

II. EXPERIMENTAL PROCEDURE

KNO_3, Al_2O_3, and H_3BO_3 were used as initial materials to fabricate glasses with a usual technique. Before synthesis Fe_2O_3 and MnO were added to the charge. Glasses were melted at 1000 and 1100 °C at oxidation conditions. The melt was poured onto steel sheets; the glass plates were naturally cooled in air down to 380 °C and kept at this temperature for several hours. The glasses were subjected to three kinds of additional thermal treatment, viz., (i) at 560 °C, (ii) at 600 °C (both during 2 h), and (iii) a two-step treatment, first at 560 then at 600 °C (during 2 h at each temperature). The MnO concentrations, as well as the synthesis and additional thermal treatment temperatures for different samples, are shown in Table I.

The FR as a function of the light wavelength and external magnetic field was measured at room temperature on optically polished samples of 0.1 ± 0.05 cm thickness. A modulation of the polarization plane of the light wave provided the FR accuracy of ± 0.2 min in the whole measurement range. The magnetic field up to 0.5 T was applied normal to the sample surface.

The Mössbauer spectra were recorded with laboratory-made equipment at room temperature with the ^{57}Co in Cr source of γ-radiation in the constant acceleration regime. The α-Fe_2O_3 standard was used to graduate the spectrometer. The samples used in the Mössbauer measurements were the same as those studied by the other techniques, i.e., contained no special additions of Fe^{57} isotope.

The EMR spectra were recorded in the temperature range from 4.2 to 300 K in the *X* band (9.46 GHz) with a Bruker EMX spectrometer equipped with an ER4112HV variable temperature unit. TEM images and selected area electron diffraction data were obtained with a JEM-2010 (JEOL) microscope (200 kV) to provide fine structural characterization of the particles dispersed in the glass matrix. The energy dispersive atomic x-ray (EDAX Co) analyzer was attached to TEM in order to determine the particle composition. The minimum EDXA spot diameter was 10 nm. Samples for the TEM studies were ground in ethanol, applied on perforated carbon substrates, attached to a standard copper grid, and placed into the microscope chamber. The glass fragments prepared in this way, as a rule, contained many particles, and signals of the basic glass components were

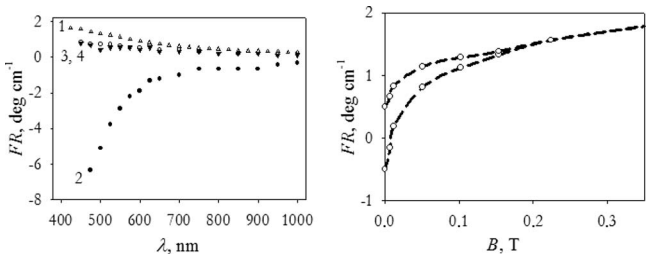

FIG. 1. Left: spectral dependences of the Faraday effect in as-prepared samples: 1—glass matrix; 2—sample 1; and 3, 4—samples 2 and 3, respectively. Right: magnetic field dependence of the FR value for as-prepared sample 1 at λ=700 nm.

present in EDXA spectra together with those of Fe and Mn. To single out separate particles, the glass fragments were dissolved in 0.1 mol NaOH solvent. This procedure removed potassium, aluminum, and boron oxides, and Mn and Fe oxide phases were dried and used for the TEM studies. Magnetization measurements as a function of temperature in the range from 5 to 300 K and the magnetic field up to 5 T were made using a Quantum Design MPMS-55 superconducting quantum interference device magnetometer with a scan length of 4 cm.

III. RESULTS AND DISCUSSION

A. As-prepared samples

1. FR

In the present case FR is the sum of two contributions: a (positive) diamagnetic rotation due to the glass matrix and a rotation due to Fe and Mn. In the case of noninteracting ions the latter contribution has negative sign; it is of paramagnetic character and is proportional to the total concentration of the paramagnetic ions. The spectral dependences of the FR are shown in Fig. 1 (left); curve 1 represents the FR values of the glass matrix with no paramagnetic additions (initial sample), and this curve is of diamagnetic character. Curves 2–4 correspond to the FR spectra of doped glasses 1–3, respectively, and include contributions of the paramagnetic ions. For samples 2 and 3 the spectral curves are shifted slightly below that of the initial sample, evidencing negative sign and smallness of the Fe and Mn ion contributions to FR. Such behavior is typical of paramagnetic FR. Equal FR values for samples 2 and 3 correspond to the equal concentrations of paramagnetic ions in the samples (Table I).

The FR spectrum of sample 1 is fundamentally distinct from those of samples 2 and 3 [see curve 2 in Fig. 1 (left)]: The FR for this sample is negative and its absolute value increases by about an order of magnitude in the shorter wavelength range, though the total amount of paramagnetic oxides in this case is even less than in samples 2 and 3. This shape of FR spectral dependence is similar to that of ferromagnetic materials containing Mn^{2+} and/or Fe^{3+} ions, such as $FeBO_3$,[24] γ-Fe_2O_3, and $MnFe_2O_4$.[25] The sharp FR increase in sample 1 infers an inhomogeneous distribution of Fe and Mn ions in the glass matrix with formation of magnetically ordered (ferromagnetic or ferrimagnetic) particles.

The latter inference is further confirmed by a nonlinear magnetic field dependence of FR for sample 1 with hysteresis, shown in Fig. 1 (right). For samples 2 and 3 the FR value is a linear function of the magnetic field up to 0.5 T. These results suggest the formation of magnetic particles in sample 1 but give no definite data on the magnetic state of paramagnetic additions in samples 2 and 3.

2. EMR

Figure 2 shows EMR spectra series of as-prepared samples 1–3 measured at different temperatures between liquid helium and room temperature. In all spectra two distinct features are observed: a low-field one with an effective g-factor $g_{ef}=4.3$ and a high-field one with $g_{ef}=2.0$. Note that the data for sample 1 show true relative spectra intensities at different temperatures while for samples 2 and 3 the intensities are multiplied by factors proportional to the absolute temperature T in order to bring out features obeying the $1/T$

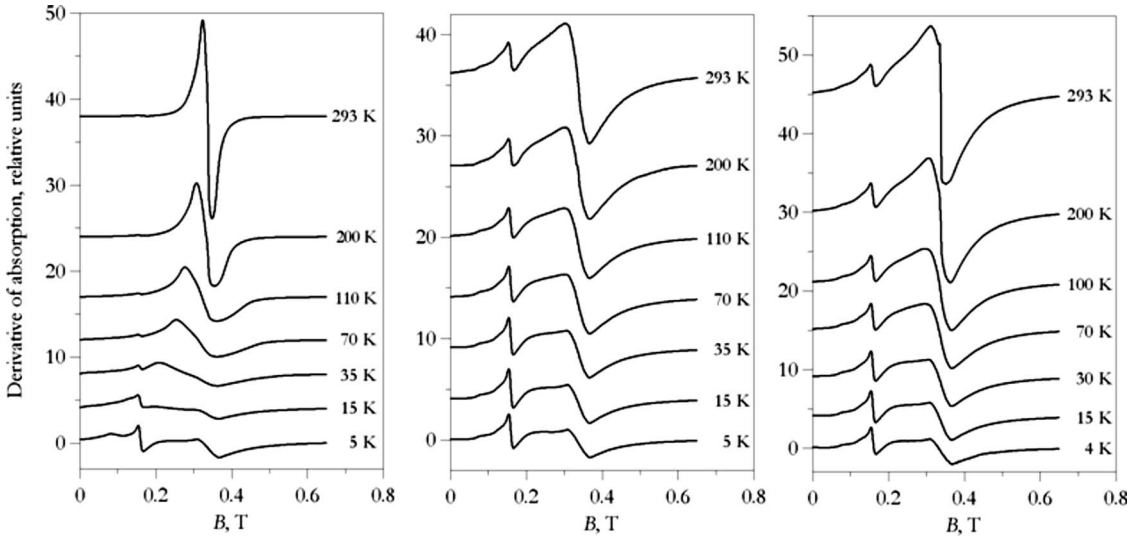

FIG. 2. Experimental EMR spectra in samples 1 (left), 2 (center), and 3 (right) at different temperatures shown alongside the curves. For sample 1 the relative intensities are plotted as measured. For samples 2 and 3 the intensity at the lowest temperatures are plotted as measured and those at higher T are multiplied, respectively, by $T/5$ and $T/4$.

Curie law characteristic of electron paramagnetic resonance (EPR) arising from diluted paramagnetic species.

One can see that the intensity of the $g_{ef}=4.3$ feature in all three samples follows the Curie law. In disordered matrices the $g_{ef}=4.3$ feature is the hallmark of $^6S_{5/2}$ ions in heavily distorted environment; in the present instance this feature can be assigned to Fe^{3+} and possibly to a part of Mn^{2+} ions diluted in the glass matrix.

In contrast, the overall intensity of the $g_{ef}=2.0$ feature does not follow the Curie law; moreover, its behavior is complex and quite different in different samples. At liquid helium temperature this feature is similar in all three samples and arises from a superposition of contributions of diluted paramagnetic ions in less distorted environment, viz., a single EPR line of Fe^{3+} and an unresolved hyperfine sextet of Mn^{2+} ions. However, the intensities of these contributions are expected to obey the Curie law, which is manifestly not the case. In the previously reported study of another borate glass system in the interval between liquid helium and room temperatures a certain increase was observed of the relative amplitude of the $g_{ef}=2.0$ feature in comparison with that of the $g_{ef}=4.3$ one and related to a decrease in the zero-field splitting parameters as temperature increases.[26] However, in the present instance this increase is much more pronounced. This behavior is most striking in sample 1 where the dramatic increase in amplitude of the $g_{ef}=2.0$ feature is accompanied with concomitant narrowing at higher temperatures. This clearly indicates the type of EMR which can be identified as the superparamagnetic resonance (SPR) of magnetically ordered nanoparticles, such as previously observed for superparamagnetic nanoparticles in thermally treated borate glasses.[12,20,26] In samples 2 and 3 the relative intensity of the $g_{ef}=2.0$ feature also increases with increasing temperature but in a less spectacular way than in sample 1. In sample 2 no perceptible change in the shape of this former feature can be noticed, while in sample 3 a distinct narrow component of this feature is developing at higher temperatures, similar to that observed in sample 1. One can conclude that the $g_{ef}=2.0$ feature arises from contributions of both diluted Fe^{3+} and Mn^{2+} ions, clusters of exchange-coupled ions, and, in sample 1 and in a lesser extent in sample 3, of magnetically ordered nanoparticles.

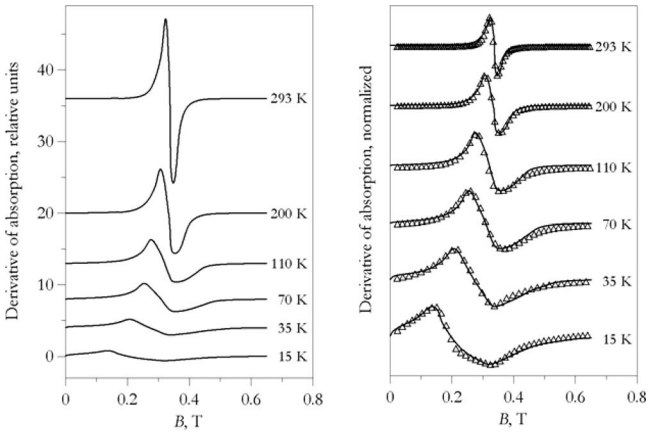

FIG. 3. Left: EMR spectra in sample 1 at different temperatures after subtracting the contributions of diluted paramagnetic ions. The relative intensities are plotted as measured. Right: computer simulations of the spectra shown on the left. Full lines: normalized experimental curves. Triangles: best-fit computer-generated spectra.

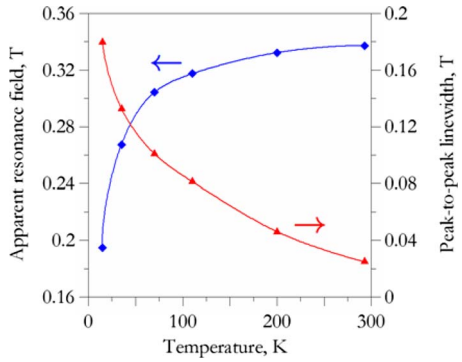

FIG. 4. (Color online) Apparent resonance field and peak-to-peak linewidth for the spectra shown in Fig. 3 (left).

In sample 1 at higher temperatures the intensity of the SPR is several orders of magnitude greater than that of the EPR of diluted ions, so, by subtracting the latter contribution from the experimental EMR spectra, the SPR contribution can be restored with sufficient accuracy. The difference spectra obtained by this procedure are shown in Fig. 3 (left). The pronounced correlation between the apparent resonance field and the peak-to-peak linewidth of these spectra (Fig. 4) is one of the distinguishing characteristics of the SPR (cf. Refs. 12 and 15).

We have carried out computer simulations of the SPR spectra series using the approach previously described in Refs. 26–28. On the basis of the FR results the nature of the nanoparticles was assumed as that of a nonstoichiometric manganese ferrite. The log-normal distribution of the nanoparticle size of the form was used. A spheroidal approximation was adopted for the nanoparticle shape, characterized by the respective demagnetizing factors $N_{\|}=\frac{1}{3}+n_{\|}$ and $N_{\perp}=\frac{1}{3}-\frac{1}{2}n_{\|}$ for nanoparticles magnetized parallel and perpendicularly to the major axes.

The best-fit computer-generated spectra are shown in Fig. 3 (right). All spectra have been obtained with one and the same joint distribution density of the nanoparticle sizes and demagnetizing factors $P\ (D,n_{\mathrm{II}})$ shown in Fig. 5 (left). From trial-and-error simulations, the accuracy of determining the distribution parameters was evaluated as being better than 10%. The marginal distribution $P\ (D)$ [see Fig. 5 (right top)] is relatively broad, with the most probable diameter of 3.2 ± 0.2 nm and the logarithmic standard deviation of diameters of 0.40 ± 0.03. The marginal distribution $P(n_{\mathrm{II}})$ [see Fig. 5 (right bottom)] shows considerable nonsphericity of statistical nature, with no particular penchant for prolate or oblate shapes.

Figure 6 shows the temperature dependences of the saturation magnetization M_s and the first-order magnetocrystalline anisotropy K extracted from the simulations. One can see that at low temperatures M_s is close to that of the bulk manganese ferrite at 0 K, $M_s\ (0)=5.6\times10^5$ A/m;[29] however, it sharply decreases with the rise of temperature, suggesting a deviation from the normal Bloch law, with exponent close to 2 instead of 3/2 and the Curie temperature T_C

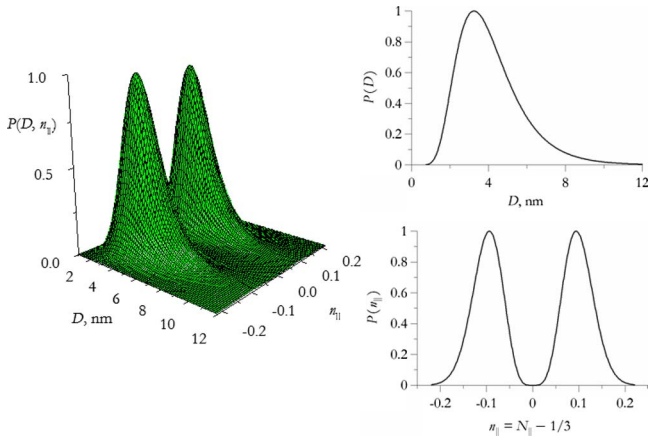

FIG. 5. (Color online) Best-fit simulation parameters for the SPR spectra in sample 1. Left: joint distribution density of diameters and demagnetizing factors. Right top: marginal distribution of diameters; right bottom: marginal distribution of demagnetizing factors.

considerably lower than in bulk manganese ferrite. Interestingly, such behavior was predicted in the mean-field calculation of finite-size effects by Hendriksen *et al.*[30] However, in the experimental studies of the temperature dependence of M_s for manganese ferrite nanoparticles, depending on the technique of preparation and thermal treatment, two opposite tendencies have been observed, viz., both a decrease[5,31] and an increase[9] in T_C with a decrease in the particle size. Both tendencies have been related to finite-size effects and/or the cation redistribution between lattice sites.

The temperature dependence of K is qualitatively quite similar to that reported in the literature for nonstoichiometric manganese ferrite $Mn_xFe_{3-x}O_4$ with $1.55 < x < 1.80$.[32] However, the absolute values of K obtained in the present study are roughly twice as large as those quoted in Ref. 32. In this context, it is worth noting that for cobalt ferrite nanoparticles the anisotropy constants also are much larger than for bulk material.[33,34]

Thus, in the glass system studied magnetically ordered clusters occur already at the first stage of the glass preparation. In particular, magnetic nanoparticles with characteristics close to those of manganese ferrite are formed for the ratio of the Fe and Mn oxides in the charge of 3:2. These results corroborate the FR data.

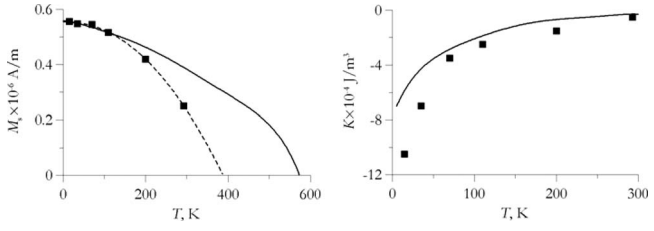

FIG. 6. Left: temperature dependence of the saturation magnetization. The full squares show the simulation results. The full curve has been calculated using the values of the saturation magnetization and the Curie temperature in Fig. 32.8 of Ref. 29. The dashed curve is the best-fit equation $M_s = 0.56 \times 10^6 (1 - T/365.5)^{1.96}$. Right: temperature dependence of the first-order anisotropy constant. The full squares are simulation results. The full curve has been calculated using that shown on the left graph and the K/M_s dependence in Fig. 11 of Ref. 30.

B. Thermally treated samples

1. FR

Under thermal treatment the character of the FR spectra of samples 2 and 3 is substantially modified; the FR becomes negative (Fig. 7), its absolute values markedly increase, and the shape of the spectral curves becomes similar to that of sample 1. In the latter sample the spectral shape remains almost unchanged, but its value sharply increases in comparison with the as-prepared sample.

One can see that the character of the modification of the FR under thermal treatment depends on the Mn concentration and the glass synthesis temperature. As far as the FR spectral dependences are similar for all treatment regimes used [Fig. 7 (left)], we can compare the FR values in different samples at one and the same wavelength. Table I shows the FR values at $\lambda = 800$ nm for each sample at different treatment temperatures. It is seen that in sample 2 a drastic FR change occurs already under treatment at 560 °C, while a treatment at 600 °C and a two-step treatment provide slightly less change. For sample 3 a treatment at 600 °C produces slightly more change in FR in comparison with that at 560 °C, and the increase in the absolute FR value is particularly pronounced for the two-step treatment. The most interesting behavior is observed in sample 1: the treatment at 560 °C leads to a spectacular FR change, which is only slightly enhanced after an additional treatment at 600 °C in the two-step process. In contrast, after a treatment directly at 600 °C the FR value remains close to that of the as-prepared sample.

The FR dependences on the external magnetic field [Fig. 7 (left)] for all thermally treated samples are similar, showing a sharp increase at relatively low fields and a slow increase at higher fields. Besides, a magnetic hysteresis is observed, the characteristics of the hysteresis loop, in particular, the relative remnant FR value α_0/α (α_0 is the FR in zero magnetic field) and, to lesser extent, the coercive field B_c correlating with the high-field FR value (Table I).

The FR values and their spectral and magnetic field dependences in the thermally treated samples are characteristics of ferromagnetic or ferrimagnetic substances having macroscopic magnetic moments. Meanwhile, because of low contents of the paramagnetic additions in the glasses, magnetic order cannot exist in the whole sample volume. The above EMR results show that magnetic nanoparticles are formed already in the as-prepared glasses. Under the thermal treatment, such fine particles can act as germs for the formation of larger magnetically ordered particles. The particle characteristics such as shape, dimensions, and structure depend on the thermal treatment regime.

Since both Fe and Mn ions are expected to be incorporated into the particles, their structure is most likely that of manganese ferrite of composition $Mn_xFe_{3-x}O_4$. The FR spectra shown in Fig. 7 confirm this assumption; indeed, as was mentioned above, in the context of the as-prepared sample 1, these spectra are very similar to those of ferrites containing $3d^5$ ions, in particular, of manganese ferrite.[25]

In Ref. 18 optical and magneto-optical properties of γ-Fe_2O_3 nanometric superparamagnetic particles frozen in

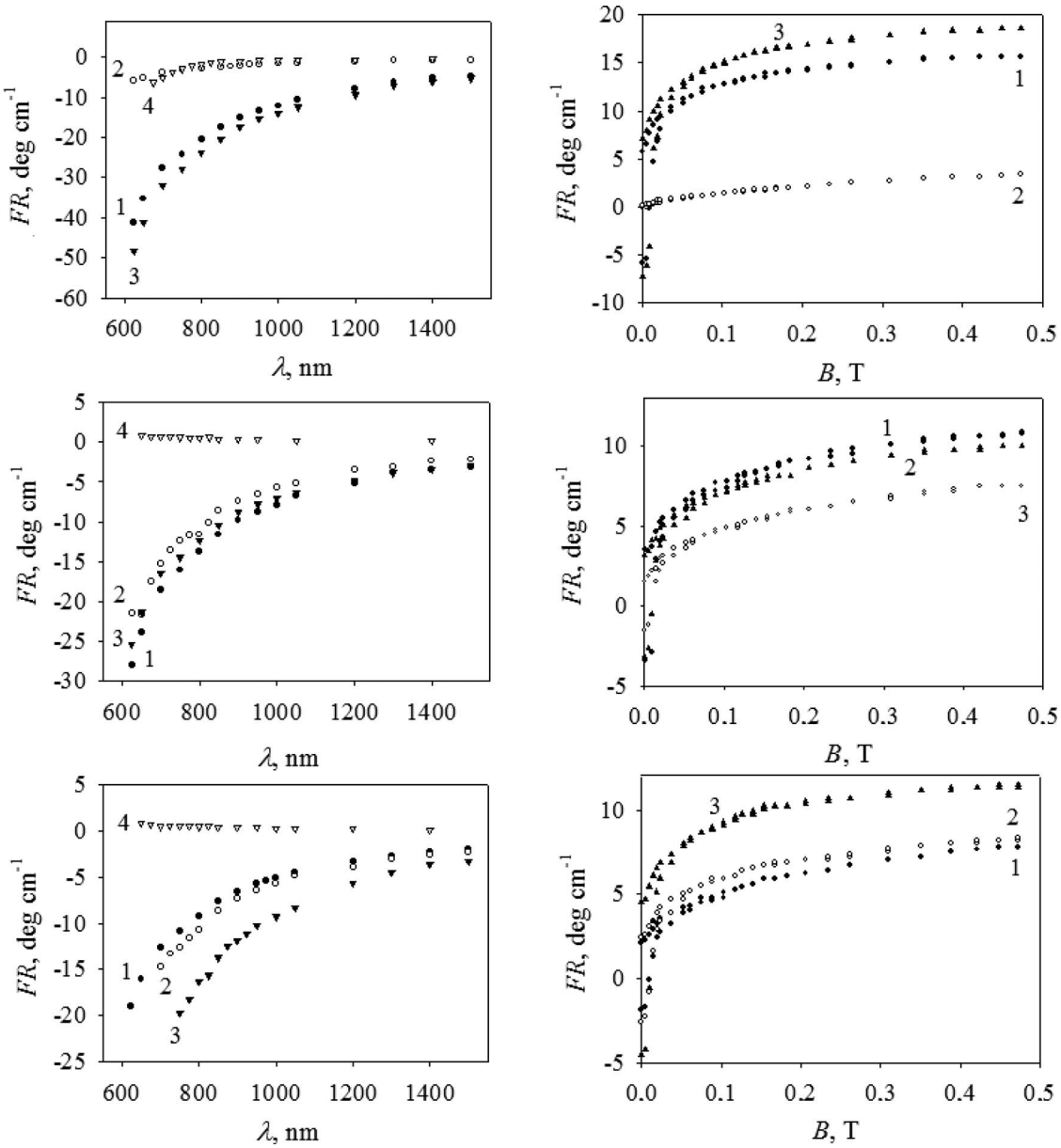

FIG. 7. Left: FR spectral dependences in the magnetic field $B=0.2$ T for the as-prepared and thermally treated samples: top—1; center—2; and bottom—3. Right: FR field dependences at the light wavelength of 925 nm for thermally treated samples: top—1; center—2; and bottom—3. The curve numbers correspond to the treatment at 1—560 °C, 2—600 °C, 3—560+600 °C, and 4—the as-prepared sample.

silica-glass matrices were studied and the material was shown to exhibit in the 1.5–2.6 eV (830–500 nm) spectral range the FR of the same order of magnitude as $Y_3Fe_5O_{12}$, a compound widely used for magneto-optical applications. Bentivegna *et al.*[18] considered this material to be very useful for applications, such as optical rotators, isolators, and modulators, based on magneto-optical principles. Our samples are not very transparent in this spectral range; on the other hand, they demonstrate promising optical and magneto-optical properties in the range of 800–1550 nm, also important for practical applications. In particular, the FR of sample 1 at 800 nm is about an order of magnitude larger than that shown in Fig. 3 of Ref. 18. Another interesting property of our glasses is a high remnant FR that allows keeping the light wave azimuth after switching off the magnetic field.

2. TEM

The TEM data confirm the idea of magnetic particle formation put forward above. Indeed, a typical TEM image of sample 1 fragments [see Fig. 8 (left)] shows the presence of

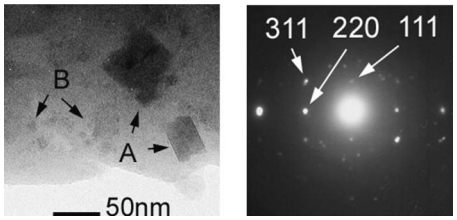

FIG. 8. Left: electron microscopy images of particles in a fragment of sample 1 (thermal treatment at 560+600 °C). Right: electron diffraction for the smaller rectangular particles marked by arrows "A" in the left part of the figure.

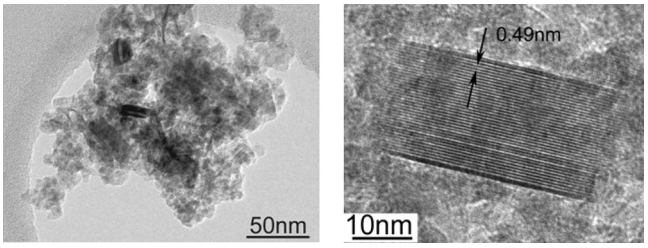

FIG. 9. Electron microscopy images of particles in sample 3 (heat treatment at 600 °C) obtained by differential dissolution of the glass matrix. Left: morphology of the particles. Right: high resolution image of different lattice zones of the large dark elongated particle shown on the left.

polydispersed nanoparticles on the background of the glass matrix. For larger particles, the electron diffraction of a selected region [Fig. 8 (right)] clearly shows a crystal structure close to that of $MnFe_2O_4$. Figure 9 illustrates the morphology of the particles in the dried concentrate of sample 3. Larger particles (up to 70 nm) of cubic habitus and ill-shaped small isolated particles are present. High resolution Transmitted Electron Microscope (TEM) images show almost perfect crystalline structure for larger particle in this case as well. The samples differ from each other in particle size distributions, the portion of larger particles increasing in the glasses having higher FR values. The EDXA spectra shown in Fig. 10 allow concluding that almost the total of Fe and Mn ions introduced into the glass are gathered inside the magnetic particles and that their concentration ratio is close to 2:1, similar to the ratio of Fe and Mn contents in bulk manganese ferrite.

The response of Fe and Mn from the particle-free glass region is very low, that of the latter being slightly higher in comparison with the former. On the basis of the EDXA data, the part of paramagnetic additions included in the particles can be estimated as approximately 85%–90% of their total amount introduced into the charge before the glass synthesis. Besides, a certain amount of Al is observed in particles separated from the matrix [Fig. 10 (bottom)].

3. Mössbauer spectra

In order to confirm the magnetic state of the nanoparticles formed in the thermally treated samples, we have studied their Mössbauer spectra. Figure 11 (left) shows typical spectra for three samples thermally treated at 560 °C and a spectrum for sample 1 subjected to the two-step treatment at 560+600 K in comparison with a spectrum of manganese ferrite single crystal. The spectra consist of a sum of Zeeman-split sextets and quadrupole doublets and differ from each other in relative intensities of the sextet and the doublet.

The overall broadness of the spectral lines, comparable intensities of inside and outside lines of the sextets, as well as the coexistence of sextets and doublets indicate superparamagnetic relaxation effects, observable as far as the measurement time of the Mössbauer effect is much longer than the superparamagnetic relaxation time of a particle, τ. In this issue, the overall shape of the Mössbauer spectra depends on the relation between τ and the lifetime τ_L of a given state of the ion.

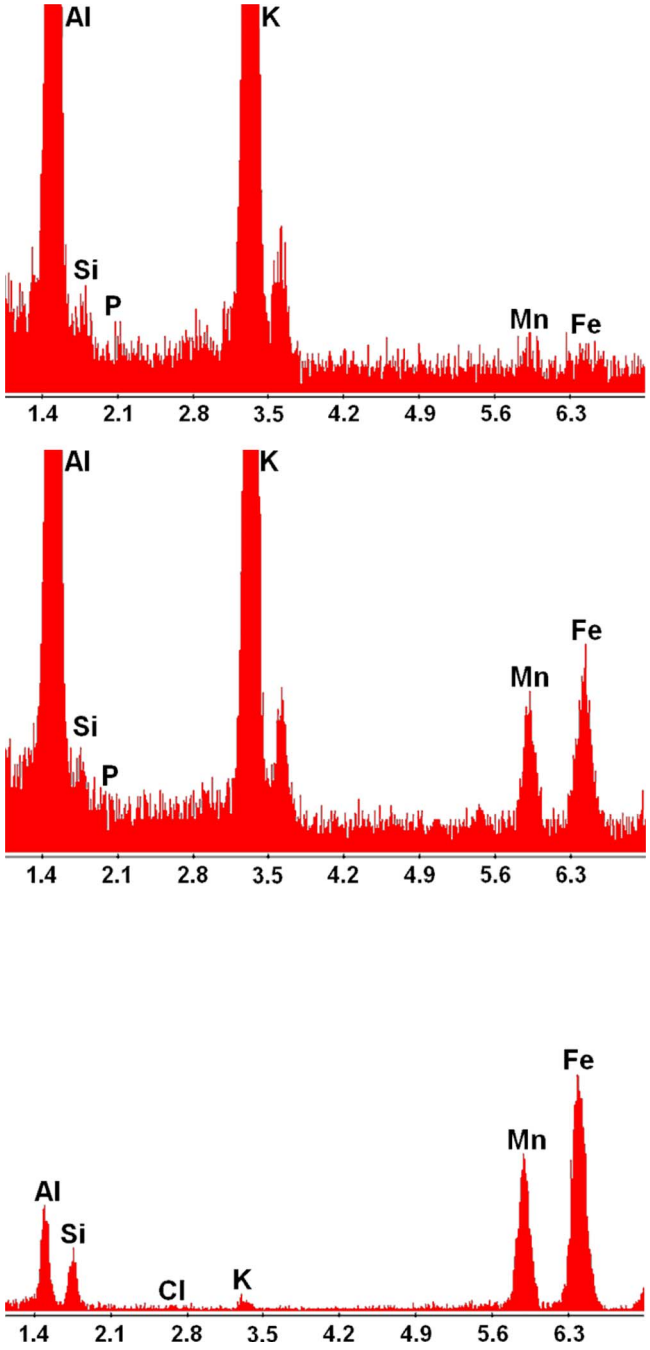

FIG. 10. (Color online) EDXA spectra for sample 1. Top—for a particle-free part of the sample; center—for particle "A" capsulated in glass [Fig. 8 (left)]; and bottom—for particles extracted by dissolution of the matrix [Fig. 9 (left)].

The distributions of hyperfine magnetic fields P (B) [Fig. 11 (center)] and quadrupole splitting P (QS) [Fig. 11 (right)] were reconstructed from the measured Mössbauer spectra. P (B) was determined by fitting the isomer chemical shift and the QS, assuming them to be the same for all sextets in a given sample. P (QS) was determined by fitting the isomer shift, assumed to be the same for all doublets in a given sample. The average hyperfine parameters are shown below the corresponding curves for each sample in Fig. 11 (center and right). The character S stands for the population of iron sites for a given distribution. The isomer shift values, given with respect to α-Fe, indicate the trivalent state of iron

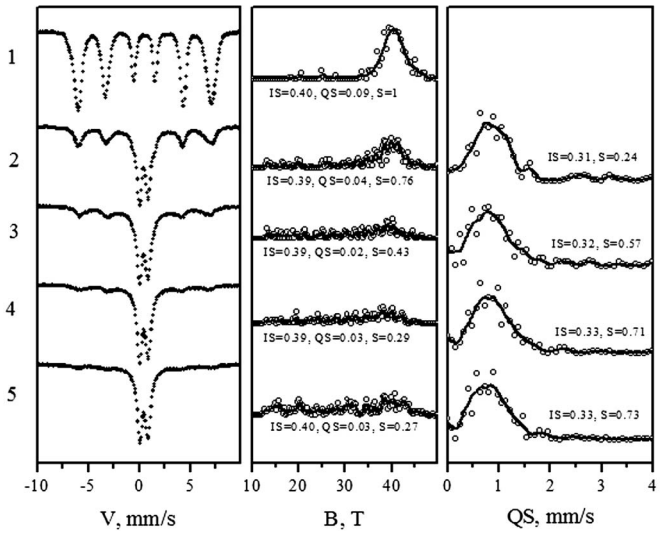

FIG. 11. Left: Mössbauer spectra; center: distribution of hyperfine fields at the iron nuclei; and right: distribution of QS in the paramagnetic part of the spectra for 1—bulk single crystal of manganese ferrite, 2—sample 1 after the two-step treatment, 3, 4, 5—samples 1, 2, 3 treated at 560 °C, respectively.

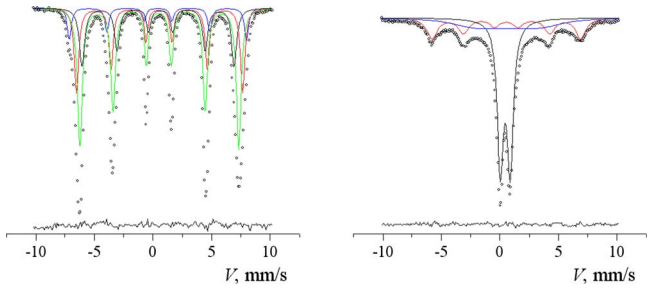

FIG. 12. (Color online) Room temperature Mössbauer spectra of bulk single crystal of manganese ferrite (left) and sample 1 subjected to two-step treatment (right). Points are the experimental data, solid lines are components of the experimental spectra (for sample 1 only some components are shown not to overload the picture), and the curves in the lower parts are differences between the experimental spectra and the sum of the components.

for all sites observed. For manganese ferrite the distribution of P (B) is rather narrow [Fig. 11 (center, curve 1)] with a maximum at approximately 42 T and the paramagnetic component in P (QS) is absent.

The features found in the P (B) and P (QS) distributions have been used to reconstruct "model" spectra, and the latter have been fitted to the experimental ones by varying the whole set of hyperfine parameters. Examples of such fitting are shown in Fig. 12 for the bulk Mn ferrite and for sample 1 subjected to the two-step thermal treatment. The fitting results for manganese ferrite and for sample 1 are shown in Table II.

In manganese ferrite four nonequivalent Fe^{3+} sites have been found. The tetrahedral (A) sites have the isomer shift about 0.26 mm/s. In the octahedral sublattice (B) three nonequivalent sites, denoted as B1, B2, and B3, arise because of a statistical distribution of Fe and Mn sites. Taking into account the populations of different sites, the cation distribution is estimated as $(Mn_{0.79}Fe_{0.21})[Mn_{0.21}Fe_{1.79}]O_4$, quite typical of manganese ferrite.[29]

The Mössbauer spectrum of sample 1 has been analyzed in an analogous way. Comparing the sextet parameters for manganese ferrite and for sample 1, one can see that for the latter the population of the octahedral sites decreases in comparison with that of the tetrahedral sites. This decrease cannot be explained by a cation redistribution, viz., substitution of iron for manganese in the tetrahedral sublattice with expulsion of the latter to the octahedral sublattice. Indeed, $Mn^{2+}(d^5)$ and $Fe^{3+}(d^5)$ have approximately equal magnetic moments; therefore, such redistribution would cause no significant changes in the hyperfine field on the iron nuclei. Meanwhile, it is seen from Table II that in sample 1 the hyperfine fields are considerably reduced in comparison with bulk manganese ferrite, this reduction being particularly pronounced for the A sites. Therefore, the observed tendency can be explained by diamagnetic dilution of ferrite. As the hyperfine field at the A sites, in the first place, "feels" the magnetic state of the B sublattice, the reduction in the former can be due to a preference toward diamagnetic dilution of the latter. Most likely, this dilution occurs because of aluminum contained in the glass entering in the ferrite nanoparticles,

TABLE II. Mössbauer parameters for bulk manganese ferrite and sample 1, subjected to two-step thermal treatment.

	Isomer shift (±0.02 mm/s)	B_{hf} (±0.5 T)	Quadrupole splitting (±0.03 mm/s)	$S \pm 0.05$	Site attribution
	0.26	469	0.03	0.07	A
	0.40	437	0.16	0.32	B1
	0.39	419	0.10	0.41	B2
Mn ferrite	0.39	401	0.37	0.20	B3
	0.25	412	0.02	0.05	A
	0.43	411	0.25	0.16	B1
	0.38	386	0.23	0.18	B2
	0.37	349	0.15	0.06	B3
	0.26	···	0.41	0.05	A
	0.31	···	0.75	0.17	B1
	0.32	···	1.08	0.18	B2
Sample 1	0.47	···	1.09	0.16	Fast-relaxing site

and Al ion is known to prefer octahedral sites in the ferrite lattice.[35,36] A possible role of size effects in the reduction in the hyperfine field on the iron nuclei is certainly less significant because in the superparamagnetic state only a slight reduction in the hyperfine field takes place up to the transition temperature.[37] The idea of the Al dilution is consistent with the EDXA data for the nanoparticles extracted from the glass matrix [Fig. 10 (bottom)].

The isomer shift values show that the paramagnetic part of the spectrum of sample 1 contains contributions of both tetrahedral and octahedral Fe ions. In contrast, no significant contribution is observed of sites with high QS typical of glass with a broad distribution of surroundings of the iron ions. Obviously, only a small part of iron remains diluted in the glass matrix, in accordance with the EDXA picture for the particle-free glass region (Fig. 10, see above). It should be noted that a satisfactory agreement between the model and the experimental spectrum can be obtained only by assuming a contribution of about 16% in intensity of a doublet with an exceptionally large linewidth (see the last line in Table II). Such doublet can be tentatively ascribed to a Fe sextet with the relaxation time of the magnetic moment comparable to the lifetime of the excited state of the Fe nucleus. In summary, the characteristics of the Mössbauer spectra in sample 1 can be explained by (i) the diamagnetic dilution manifesting itself in the presence of sextets with low hyperfine splitting and (ii) the superparamagnetic relaxation occurring for fine manganese ferrite nanocrystals at room temperature.

In the spectra of samples 1–3 subjected to one-step thermal treatment in comparison with that of sample 1 subjected to two-step treatment (Fig. 11) the contribution of the sextets decreases while that of the paramagnetic doublets increases. Therefore, in these samples the portion of ferrite nanoparticles in ferrimagnetic state decreases while the particle-free portion increases. This behavior shows that in the series of samples 1–3, the effective nanoparticle size decreases, stimulating the superparamagnetic transition. The diamagnetic dilution, which manifests itself in the presence of sextets with low hyperfine fields, facilitates the transition to the superparamagnetic state. The "smearing" of sextets throughout the whole range of hyperfine fields in sample 3 can be explained by the presence of an assembly of ferrite nanoparticles with broad variations in the degree of diamagnetic dilution. The populations corresponding to the paramagnetic parts of the Mössbauer spectra show a preference of iron in aluminum borate glasses for joining the ferrite particles; indeed, 70%–75% of the total iron amount is contained in the particles and only 25%–30% of iron ions are diluted in the glass matrix.

In conclusion, the Mössbauer spectroscopy confirms the finding that the particles formed in thermally treated glass samples possess magnetic order similar to that of the bulk manganese ferrite, at least for larger-sized particles. At room temperature a considerable part of the particles is in superparamagnetic state.

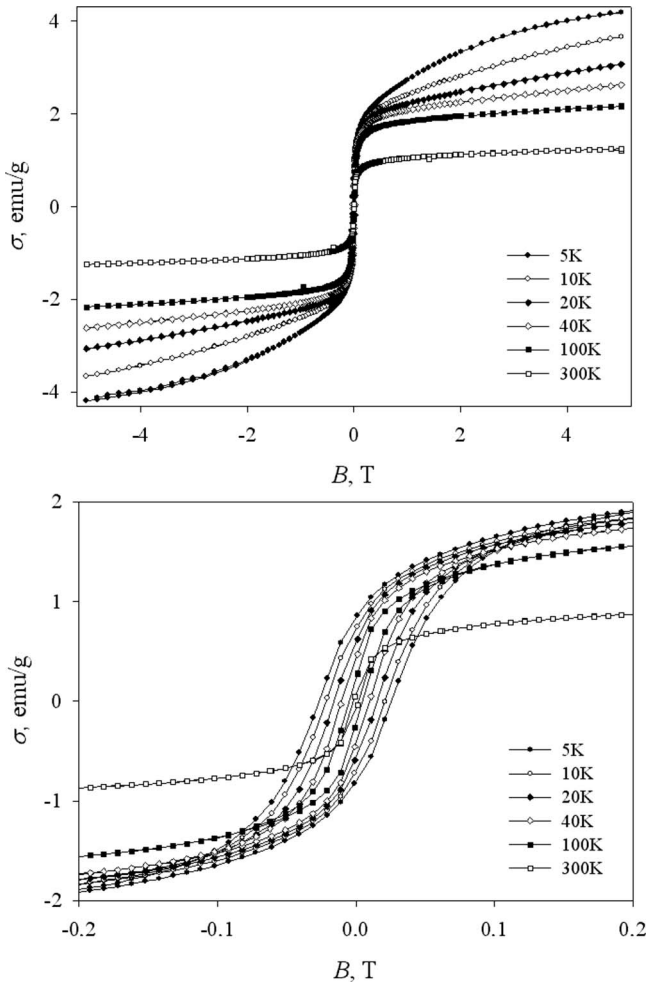

FIG. 13. Magnetization curves for sample 1 at different temperatures in the magnetic fields of 5 T (top) and 0.2 T (bottom). The magnetization value refers to the whole sample mass.

4. Field and temperature dependences of the magnetization

The set of magnetization curves taken at different temperatures is shown in Fig. 13 (top) for sample 1 subjected to two-stage thermal treatment at 560+600 °C. The electron microscope image and the Mössbauer spectrum of this sample are shown, respectively, in Figs. 8 and 11 (curve 2). Note that for all samples the shape of the magnetization curves is very close to that of the magnetic field dependences of the FR, as expected since the latter is a linear function of magnetization. The magnetization curve at room temperature is typical of soft ferromagnets, but magnetic saturation is not achieved even at 5 T. The field region where the magnetization shape changes from rapid to slow increase with an increase of magnetic field corresponds to 0.1–0.3 T for different samples. These room temperature curves are very close to those reported for $MnFe_2O_4$ powder[11] and nearly defect-free powdered maghemite nanocrystals.[4] However, the magnetization curves observed in Refs. 4 and 11 did not change when temperature decreased to 5 K. Quite different temperature behavior is characteristic of the glass samples studied in the present work. The shape of the magnetization curves remains unchanged in the temperature range from 300 down to

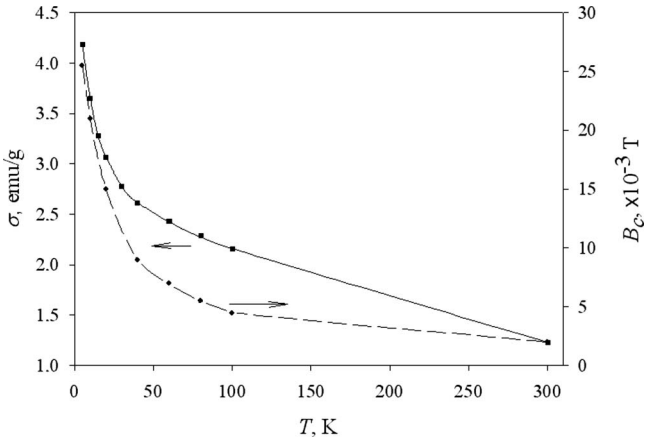

FIG. 14. Temperature dependences of the magnetization in magnetic field 5 T and coercive field for sample 1.

approximately 100 K; the low-field and high-field magnetic susceptibilities do not change either, but the value of the magnetization significantly increases.

A further decrease in temperature (below 100 K) results in an increase in the high-field susceptibility. The hysteresis loops in the low-field range shown in Fig. 13 (bottom) broaden with the decrease in temperature. The temperature dependence of magnetization measured in the magnetic field of 5 T and that of the coercive field for sample 1 are shown in Fig. 14. Both the set of low temperature (below 100 K) magnetization curves shown in Fig. 13 (top) and the temperature dependence of magnetization are very similar to those observed[6] for noninteracting γ-Fe_2O_3 nanoparticles (of 2.7 nm in size) dispersed in polyvinyl alcohol. Note however that the γ-Fe_2O_3 particles of same size in the powdered state demonstrated no temperature changes of magnetization curves.[6]

In spite of certain variations from sample to sample, the general behavior of the magnetic characteristics observed is quite similar in all samples, and it can be explained by a statistical distribution in the nanoparticle size. At room temperature larger particles are already "frozen" and provide magnetization curves of ferromagnetic type, while the contribution of smaller particles is negligible. As temperature decreases, the size effects in smaller particles become more and more important, so the character of the magnetization curve is considerably changed (for instance, cf. Ref. 6). The increase in the coercive field with a decrease in temperature can be due, on the one hand, to an increase in magnetic anisotropy of manganese ferrite[32] and, on the other hand, to an increase of the contribution of frozen particles.

The magnetization values in Figs. 13 and 14 refer to the total mass of the samples; indeed, the mass of the particles in each sample is not exactly known. Meanwhile, on the basis of the mass concentration of the paramagnetic oxides introduced in the glasses and the EDXA data we can estimate the magnetization proper to the particles. For instance, for sample 1 the magnetizations in the highest magnetic field used (5 T) are approximately 28 emu/g at 300 K and approximately 102 emu/g at 5 K. Comparing these values with those of bulk manganese ferrite,[29] we see that the nanoparticle magnetization at 300 K is several times lower than in bulk manganese ferrite, 80 emu/g, while at low temperatures it approaches the magnetization of the latter, 112 emu/g at 0 K. The above conjecture on the predominant contribution to the magnetization of larger nanoparticles at higher temperatures and of smaller nanoparticles at lower temperatures results in an estimate of the mass portion of larger particles of approximately 30%.

5. EMR

The heat treatment brings drastic changes in the EMR spectra (see Fig. 15). For all samples the g_{ef}=2.0 and g_{ef} =4.3 features due to diluted Fe^{3+} and Mn^{2+} ions disappear, and the spectra acquire the characteristic of SPR of a nanoparticle assembly.[20,26] In particular, the superparamagnetic

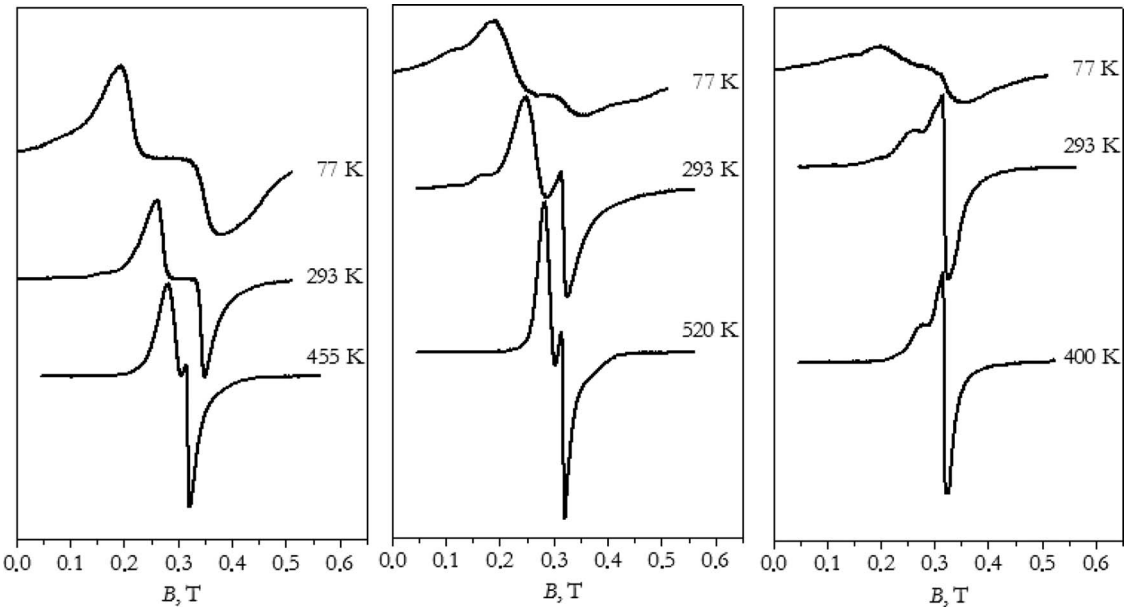

FIG. 15. Experimental EMR spectra in samples 1 (left), 2 (center), and 3 (right) treated at 560+600 °C, recorded at different temperatures shown alongside the curves. The relative intensities are plotted as measured.

nature of the EMR spectra is attested by the spectacular temperature-induced narrowing of the spread in the resonance magnetic fields.

A qualitative comparison between the EMR spectra in the as-prepared, *vide supra*, and the annealed glasses indicates much larger average size and distribution of the morphological characteristics of the magnetic particles in the latter case. This distinction can be explained by the fact that in the course of the thermal treatment the diluted paramagnetic ions are both joining already existing nanoparticles and forming new ones. The EMR data for the thermally treated samples are in accordance with those of TEM and the Mössbauer effect. Computer simulations of the EMR spectra of the thermally treated samples are in progress, and the corresponding results will be published elsewhere.

IV. SUMMARY

FR, EMR, TEM, Mössbauer spectroscopy, and magnetic measurements of as-prepared and thermally treated potassium-aluminum-boron glasses doped with low concentrations of Fe and Mn oxides have been studied. In spite of very low contents of the paramagnetic ions, clustering and magnetic ordering occur already at the first stage of the glass preparation. In particular, magnetic nanoparticles with characteristics close to those of manganese ferrite are formed for the ratio of the Fe and Mn oxides in the charge of 3:2.

The glasses subjected to an additional thermal treatment clearly demonstrate magnetic and magneto-optical properties typical of magnetically ordered materials. In the course of the treatment, already existing clusters and fine nanoparticles act as germs for the formation of larger magnetically ordered particles. The formation of such particles has been directly confirmed by the TEM. The particle characteristics such as shape, dimensions, and structure depend on the thermal treatment regime. The larger particles are shown to be crystalline.

The EMR data in the as-prepared glasses show a coexistence of diluted paramagnetic ions, clusters, and fine nanoparticles. In the thermally treated glasses larger magnetic nanoparticles are formed, giving rise to the SPR spectra. The Mössbauer spectroscopy confirms the manganese ferrite structure of the nanoparticles formed in the thermally treated glasses as well as the superparamagnetic state of these particles. The magnetic field and temperature dependences of the magnetization for the nanoparticle assembly in the glass are similar to the analogous characteristics for powdered ferrite nanoparticles at higher temperatures and for dispersed ferrite nanoparticles at lower temperatures. Such behavior is explained by morphological and spatial distribution of the particles in the glass matrix. In summary, the main advantages of the glass system studied in this work are high FR in the near infrared spectral range at relatively low magnetic field, presence of the remnant rotation, and compatibility of this material with glassy elements of various optical devices.

ACKNOWLEDGMENTS

A financial support from the Russian Foundation for Basic Research (RFBR)-CNRS (Grant No.07-02-92174) is highly appreciated. R. Ivantsov is grateful to the Russian Science Support Foundation. Y. Yeshurun acknowledges the support of the Israel Scienc Foundation (ISF).

[1] C. R. Vestal and Z. J. Zhang, J. Am. Chem. Soc. **125**, 9828 (2003).
[2] J. Wang, C. Zeng, Z. M. Peng, and Q. W. Chen, Physica B **349**, 124 (2004).
[3] R. H. Kodama and A. E. Berkovitz, Phys. Rev. B **59**, 6321 (1999).
[4] P. Dutta, M. S. Seehra, N. Shan, and G. P. Huffman, Phys. Rev. B **70**, 174428 (2004).
[5] J. P. Chen, C. M. Sorensen, K. I. Klabunde, G. C. Hadjipannayis, E. Devlin, and A. Kostikas, Phys. Rev. B **54**, 9288 (1996).
[6] E. Tronc, A. Ezzir, R. Cherkaoui, C. Chaneac, M. Nogues, H. Kachkachi, D. Fiorani, A. M. Testa, J. M. Greneche, and J. P. Jolivet, J. Magn. Magn. Mater. **221**, 63 (2000).
[7] M. A. Ahmed, N. Okasha, and S. I. El-Dek, Nanotechnology **19**, 065603 (2008).
[8] D. Fiorani, A. M. Testa, E. Tronc, F. Lucari, F. D'Orazio, and M. Nogues, J. Magn. Magn. Mater. **226–230**, 1942 (2001).
[9] M. Zheng, X. C. Wu, B. S. Zou, and Y. J. Wang, J. Magn. Magn. Mater. **183**, 152 (1998).
[10] J. L. Dormann, D. Fiorani, and E. Tronc, J. Magn. Magn. Mater. **202**, 251 (1999).
[11] M. Muroi, R. Street, P. G. McCormick, and J. Amighian, Phys. Rev. B **63**, 184414 (2001).
[12] R. Berger, J.-C. Bissey, J. Kliava, and B. Soulard, J. Magn. Magn. Mater. **167**, 129 (1997).
[13] K. Mandal, S. Chakraverty, S. Pan Mandal, P. Agudo, M. Pal, and D. Chakravorty, J. Appl. Phys. **92**, 501 (2002).
[14] N. Rezlescu and L. Rezlescu, Mater. Sci. Eng., A **375–377**, 1273 (2004).
[15] J. Kliava and R. Berger, in *Smart Materials for Ranging Systems*, edited by J. Franse (Springer, Berlin, 2006), pp. 27–48.
[16] G. W. Day and A. H. Rose, Proc. SPIE **985**, 138 (1988).
[17] G. E. Lano and C. Pinyan, Laser Focus World **31**, 125 (1995).
[18] F. Bentivegna, M. Nyvlt, J. Ferre, J. P. Jamet, A. Brun, S. Visnovsky, and R. Urban, J. Appl. Phys. **85**, 2270 (1999).
[19] T. W. Cease, J. G. Driggans, and S. J. Weikel, IEEE Trans. Power Deliv. **6**, 1374 (1991).
[20] R. Berger, J. Kliava, and J.-C. Bissey, J. Appl. Phys. **87**, 7389 (2000).
[21] R. Berger, J.-C. Bissey, J. Kliava, H. Daubric, and C. Estournes, J. Magn. Magn. Mater. **234**, 535 (2001).
[22] I. Edelman, R. Ivantsov, A. Vasiliev, S. Stepanov, E. Kornilova, and T. Zarubina, Physica B **301**, 203 (2001).
[23] J. Kliava, A. Marbeuf, I. Edelman, R. Ivantsov, O. Ivanova, E. Petrakovskaja, S. A. Stepanov, and V. I. Zaikovskii, Proceedings of the 21st International Congress on Glass, Strasbourg, Proceedings No. A24, 2007 (unpublished), p. 4.
[24] I. S. Edelman and A. V. Malakhovskii, Opt. Spectrosc. **35**, 959 (1973).
[25] Z. Šimša, P. Tailhades, L. Presmanes, and C. Bonningue, J. Magn. Magn. Mater. **242–245**, 381 (2001).
[26] J. Kliava and R. Berger, *Recent Research Development In Non-Crystalline Solids* (Transworld Research Network, Trivandrum, India, 2003), Vol. 3, p. 41.
[27] J. Kliava and R. Berger, J. Magn. Magn. Mater. **205**, 328 (1999).
[28] J. Kliava, A. Malakhovskii, I. Edelman, A. Potseluyko, E. Petrakovskaja, S. Melnikova, T. Zarubina, G. Petrovskii, I. Bruckental, and Y. Yeshurun, Phys. Rev. B **71**, 104406 (2005).
[29] J. Smit and H. P. J. Wijn, *Ferrites*, N. V. Philips, ed., (Philips Technical Llibrary, Eindhoven, The Netherlands, 1959).
[30] P. V. Hendriksen, S. Linderoth, and P.-A. Lindgård, J. Magn. Magn. Mater. **104–107**, 1577 (1992).
[31] C. Tsang, H. D. Gafney, D. Sunil, M. Rafailovich, J. Sokolov, and R. J. Gambino, J. Appl. Phys. **79**, 6025 (1996).
[32] W. Palmer, Jpn. J. Appl. Phys., Suppl. **33**, 1201 (1962).
[33] L. D. Tung, V. Kolesnichenko, D. Caruntu, N. H. Chou, C. J. O'Connor, and L. Spinu, J. Appl. Phys. **93**, 7486 (2003).
[34] A. Virden, S. Wells, and K. O'Grady, J. Magn. Magn. Mater. **316**, e768 (2007).
[35] S. Krupicka, *Physik der Ferrite und der Verwandten Magnetischen Oxide* (Academia Verlag der Tsechoslovakischen Academie der Wissenschaften, Prag, 1973).
[36] V. I. Maltsev and E. P. Najden, Crystallogr. Rep. **28**, 870 (1983) (in Russian).
[37] I. P. Suzdalev, *Dynamic Effects in Gamma-Resonance Spectroscopy* (Atomizdat, Moscow, 1979).